Liver Research 9 (2025) 298–312

Contents lists available at ScienceDirect

Liver Research

journal homepage: http://www.keaipublishing.com/en/journals/liver-research

Original Article

Cancer cachexia-related monocytic myeloid-derived suppressor cells impair T-cell negative selection and predict immune-related adverse events

Li Wei [a,b,1], Ya-Qin Sun [a,1], Jian-Hua Ren [c,1], Ze-Xuan Huang [b], Yuan Zhang [d], Xiu-Qing Pang [b,e], Xiao-Tong Lv [a,b], Xiang-Yuan Wu [a,b,*], Yan-Fang Xing [f,**], Xing Li [a,g,***]

[a] Department of Medical Oncology, The Third Affiliated Hospital of Sun Yat-sen University, Guangzhou, Guangdong, China
[b] Guangdong Key Laboratory of Liver Disease Research, The Third Affiliated Hospital of Sun Yat-sen University, Guangzhou, Guangdong, China
[c] Department of Articular Surgery, The Third Affiliated Hospital of Sun Yat-sen University, Guangzhou, Guangdong, China
[d] Department of Obstetrics, The Third Affiliated Hospital of Sun Yat-sen University, Guangzhou, Guangdong, China
[e] Department of Infectious Diseases, The Third Affiliated Hospital of Sun Yat-sen University, Guangzhou, Guangdong, China
[f] Department of Nephrology, The Third Affiliated Hospital of Guangzhou Medical University, Guangzhou, Guangdong, China
[g] Department of Medical Examination Center, The Third Affiliated Hospital of Sun Yat-sen University, Guangzhou, Guangdong, China

ARTICLE INFO

Article history:
Received 23 April 2025
Received in revised form
10 July 2025
Accepted 10 October 2025

Keywords:
Cancer cachexia
Thymus involution
T-cell negative selection
Monocytic myeloid-derived suppressor cells (M-MDSCs)
Immune-related adverse events (irAEs)
Anti-PD-1/L1 therapy

ABSTRACT

Background and aims: Cancer cachexia is prevalent in various cancers and is associated with chemotherapy toxicity. However, limited data exist on the relationship between cachexia and immune-related adverse events (irAEs). The aim of this study is to explore the correlation between cancer cachexia and irAEs and its possible mechanism.

Methods: A murine model of orthotopic hepatocellular carcinoma (HCC) with cachexia was developed to evaluate the impact of T-cell infiltration into multiple tumor-free organs on the occurrence of irAEs. Single-cell RNA sequencing of thymic stromal cells was performed. Additionally, patients with advanced cancers receiving anti-programmed cell death protein 1/ligand 1 (PD-1/L1) antibody treatment were followed to investigate the relationship between cachexia and irAEs.

Results: Inflammatory cell infiltration was observed in multiple tumor-free organs of cachexic HCC mice but not in non-cachexic controls. Immunofluorescence confirmed that the infiltrating cells included $CD4^+$ and $CD8^+$ T cells. Morphological assessment and hematoxylin–eosin staining revealed thymic atrophy in cachexic HCC mice. Single-cell RNA sequencing of thymic stromal cells showed a reduction in medullary thymic epithelial cells (mTECs) II and III in cachexic mice. Autoimmune regulator (Aire) downregulation was accompanied by decreased expression of tissue-restricted antigens in mTECs. T cells from cachexic HCC mice induced organ-specific inflammation and T-cell infiltration in multiple organs of tumor-free mice. Following anti-mouse PD-1 antibody treatment, the incidence of inflammation in multiple organs markedly increased in cachexic HCC mice and in tumor-free mice that had received T cells from the cachexic HCC mice. Flow cytometry and immunofluorescence analyses revealed enrichment of thymic monocytic myeloid-derived suppressor cells (M-MDSCs) in cachexic HCC mice. M-MDSCs infiltrated the thymus in cachexic mice with cancer, and they induced apoptosis of mTECs from tumor-free mice *in vitro* via nitric oxide production. Transfer of M-MDSCs led to inflammatory cell infiltration in multiple organs and thymic involution in tumor-free mice without affecting body weight.

* Corresponding author. Department of Medical Oncology and Guangdong Key Laboratory of Liver Disease Research, The Third Affiliated Hospital of Sun Yat-sen University, Guangzhou, Guangdong, China.
** Corresponding author. Department of Nephrology, The Third Affiliated Hospital of Guangzhou Medical University, Guangzhou, Guangdong, China.
*** Corresponding author. Department of Medical Oncology and Medical Examination Center, The Third Affiliated Hospital of Sun Yat-sen University, Guangzhou, Guangdong, China.
E-mail addresses: wuxiangy@mail.sysu.edu.cn (Xiang-Yuan Wu), 2574410512@qq.com (Yan-Fang Xing), lixing9@mail.sysu.edu.cn (Xing Li).
Peer review under the responsibility of Editorial Office of Liver Research.
[1] These authors contributed equally to this work.

https://doi.org/10.1016/j.livres.2025.10.001
2542-5684/© 2025 The Third Affiliated Hospital of Sun Yat-Sen University. Publishing services by Elsevier B.V. on behalf of KeAi Communications Co. Ltd. This is an open access article under the CC BY-NC-ND license (http://creativecommons.org/licenses/by-nc-nd/4.0/).

Sixty-four patients with advanced cancer receiving anti-PD-1/L1 therapy were enrolled. Patients who developed irAEs had higher levels of circulating M-MDSCs than those who did not. Moreover, patients with cachexia (body mass index (BMI) < 20 kg/m^2 or ≥5% weight loss over the past 6 months) had elevated M-MDSC levels. Patients with both high M-MDSC levels and low BMI or weight loss ≥5% experienced more irAEs (hazard ratio: 2.333; 95% confidence interval: 1.231–4.423).

Conclusions: M-MDSCs in cachexic mice induced mTEC apoptosis through nitric oxide production, impairing T-cell negative selection and promoting autoimmune T-cell infiltration into tumor-free organs. Cancer cachexia-related M-MDSCs may serve as predictive biomarkers for irAEs in patients with advanced cancer.

© 2025 The Third Affiliated Hospital of Sun Yat-Sen University. Publishing services by Elsevier B.V. on behalf of KeAi Communications Co. Ltd. This is an open access article under the CC BY-NC-ND license (http://creativecommons.org/licenses/by-nc-nd/4.0/).

1. Introduction

Although immune checkpoint inhibitors (ICIs), including antibodies targeting programmed cell death protein 1/ligand 1 (PD-1/L1), effectively boost the immune system,[1] they may also cause immune-related adverse events (irAEs).[2] The occurrence, affected organs, and severity of irAEs are difficult to predict, as they can arise in any organ system at any point during the treatment cycle and may involve multiple organs simultaneously.[3] Because irAEs can be life-threatening in some patients,[4] the ability to predict them before onset is clinically important. However, reliable predictive biomarkers and risk factors for irAEs have not yet been established.[5,6] Activated T-cell infiltration of tissues is a hallmark of irAEs,[7,8] but it remains unclear whether this is a prerequisite for irAEs development or a downstream consequence.[9]

Cachexia occurs in up to 70% of patients with cancer and contributes to at least 20% of cancer-related deaths.[10,11] Patients with pancreatic, gastroesophageal, liver, and bile duct cancers are at higher risk of developing cachexia.[12] In hepatocellular carcinoma (HCC), cachexia is prevalent across all stages, occurring in 23.7% of patients at diagnosis and in 19.0%, 23.5%, 34.7%, and 34.0% of patients with Barcelona clinic liver cancer stage 0/A, B, C, and D, respectively.[13,14] Pretreatment cachexia has been associated with chemotherapy toxicity in several cancer types, including esophageal, gastrointestinal, pancreatic, breast, and lung cancers.[15] However, the relationship between cancer cachexia and irAEs has not been previously investigated. In cachexic cancer mouse models, the thymus has been shown to exhibit significant weight loss and atrophy.[16]

We hypothesized that thymic atrophy leads to a reduction in both the number and proportion of medullary thymic epithelial cells (mTECs), which in turn express lower levels of tissue-restricted antigens (TRAs). This may result in the infiltration of activated T cells into multiple organs, potentially contributing to the development of irAEs. In this study, we investigated the role of activated T-cell infiltration in the occurrence of irAEs in tumor-free organs and examined the causal relationship between thymic atrophy and cachexia in cancer-bearing mice. We also explored the underlying mechanisms and potential clinical implications.

2. Materials and methods

2.1. Ethical approval

This study was approved by the Ethics Committee of The Third Affiliated Hospital of Sun Yat-sen University (No. RG2023-034-01) and conducted in accordance with the principles of the Declaration of Helsinki. Written informed consent was obtained from all participants prior to sample collection. All animal experiments complied with the ARRIVE guidelines and were performed in accordance with the National Research Council's Guide for the Care and Use of Laboratory Animals. Due to limited animal experimental facilities in our institution, the research team conducted careful investigations and decided to carry out the animal experiments at Ruiye model animal (Guangzhou) Biotechnology Co., Ltd (Guangzhou, China), which possesses the qualifications for animal breeding. Therefore, animal protocols were approved by the Experimental Animal Ethics Committee of Ruiye model animal (Guangzhou) Biotechnology Co., Ltd (No. RYEth20220413-1).

2.2. Cell lines

The murine hepatoma cell lines Hepa1-6 (#CL-0105, RRID: CVCL_0327) and B16 (#CL-0029, RRID: CVCL_F936) were obtained from Procell Life Science & Technology Co., Ltd. (Wuhan, China). Hepa1-6 cells were cultured in Dulbecco's Modified Eagle's Medium (DMEM; Gibco, Thermo Fisher Scientific, Waltham, MA, USA), and B16 cells were cultured in Roswell Park Memorial Institute-1640 medium (Gibco, Thermo Fisher Scientific, Waltham, MA, USA). Both media were supplemented with 10% fetal bovine serum (Gibco, Thermo Fisher Scientific, Waltham, MA, USA) and 1% penicillin–streptomycin (Gibco, Thermo Fisher Scientific, Waltham, MA, USA) and maintained at 37 °C in a humidified atmosphere containing 5% CO_2. Cell lines were authenticated by surface antigen profiling and routinely tested for mycoplasma contamination.

2.3. Orthotopic HCC model in mice

Male C57BL/6J and C57L/J mice (6 weeks old, weighing 20–22 g) were purchased from the Laboratory Animal Center of Sun Yat-sen University (Guangzhou, China) and housed under pathogen-free conditions. Mice were randomly assigned to experimental or control groups. Hepa1-6 cells in the logarithmic growth phase were harvested and prepared as a mixture containing 1×10^6 cells in 10 μL of phosphate-buffered saline (PBS) (Servicebio, Wuhan, China) and 10 μL of Matrigel (BD BioCoat, Corning, NY, USA).

The mice were anesthetized by intraperitoneal injection of 160 μL of 1% pentobarbital (Chenxue Biotechnology Co., Ltd., Guangzhou, China) per 25 g of body weight. Once a mouse exhibited slow, shallow breathing and no response to pain, it was secured to the lid of a 100-mm Petri dish (Servicebio, Wuhan, China), and the surgical site was sterilized. A sagittal incision approximately 1 cm in length was made in the mid-abdomen using ophthalmic scissors (Zhongke Life Science Research Co., Ltd., Guangzhou, China). The median liver lobe was gently exteriorized using a cotton swab moistened with normal saline and placed on the outer surface of the peritoneum. Then, 20 μL of the Hepa1-6 cell suspension was slowly injected under the capsule into the left lobe of the liver using a 0.5 mL insulin syringe (Becton,

Dickinson and Company, Franklin Lakes, New Jersey, USA). After injection, the needle was withdrawn, and pressure was applied with a cotton swab for 1 min to control bleeding. The liver was then returned to the abdominal cavity, and both the peritoneum and skin were closed with intermittent 5-0 sutures. The mice were placed in a lateral recumbent position on a thermal blanket (Zhongke Life Technology Co., Ltd., Guangzhou, China) until recovery from anesthesia. Control group mice underwent the same surgical procedure but were injected with 10 μL of PBS and 10 μL of the Matrigel (BD BioCoat) mixture.

After the operation, both the experimental and control groups were fed normally, and body weights were recorded every 2–3 days. Based on changes in body weight, tumor-bearing mice were classified into two groups: those with <5% weight loss (HCC without cachexia; $n = 6$) and those with 5%–10% weight loss (HCC with cachexia; $n = 6$) compared with tumor-free mice (sham-operated group; $n = 6$).

2.4. Murine subcutaneous tumor models

Routinely cultured Hepa1-6 cells and B16 cells at the logarithmic growth stage were digested and prepared as a cell suspension containing 1×10^7 cells/mL PBS. The middle and posterior armpits were selected as the injection points and disinfected with 75% ethanol (Servicebio, Wuhan, China). Before inoculation, the cell suspension was mixed well with a 200 μL pipette; 100 μL of the cell suspension was injected subcutaneously. Post-inoculation, the mice were fed normally, and the longest tumor was measured with a vernier caliper every 3–4 days. The shortest diameter line (mm), tumor volume (mm^3), and mouse weight (g) were recorded.

2.5. Single-cell RNA sequencing (scRNA-seq) and data analysis

Fresh $CD45^-$ thymic cells were isolated using the EasySep™ Mouse CD45 Positive Selection Kit (Stemcell Technologies, Vancouver, Canada). scRNA-seq was performed using the Chromium Single Cell platform (10 × Genomics, Pleasanton, CA, USA). Cell viability was assessed using trypan blue exclusion and dual-fluorescence staining with acridine orange and propidium iodide.

Cell Ranger software (version 6.0.1; 10 × Genomics) was used for demultiplexing, genome alignment (GRCh38), barcode counting, and unique molecular identifier counting of the raw sequencing data. Seurat (version 4.0.0) was employed for quality control, normalization, dimensionality reduction, clustering, and visualization of the raw count matrix. A total of 6531 single cells from six tumor-free mice and 7046 cells from six cachexic HCC mice were included in the final analysis.

Principal component analysis was performed to reduce feature dimensionality using the *RunPCA* function. The first 20 principal components, with a resolution parameter of 0.6, were used to identify clusters via the *FindClusters* function. Dimensionality reduction was then visualized using uniform manifold approximation and projection with the *RunUMAP* function. Cytokine expression matrices were extracted for differential analysis between normal and tumor samples using the ggpubr package in R. Gene sets related to cell death pathways were obtained from the Kyoto Encyclopedia of Genes and Genomes (KEGG), MSigDB, and FerrDb V2 databases and analyzed using the clusterProfiler, msigdbr, and ggpubr packages in R, respectively.

2.6. Study participants

Patients with advanced cancer who received anti-PD-1/L1 antibody (Supplemental Table 1) treatment at The Third Affiliated Hospital of Sun Yat-sen University between January 1 and December 31, 2022, were included in this study (Supplemental Table 1). Additional inclusion criteria were as follows: (i) age ≥18 years and <80 years; (ii) pathological confirmation of an advanced malignant tumor; and (iii) clinical indication for anti-PD-1/L1 antibody treatment.

Exclusion criteria were (i) pregnancy or lactation; (ii) mental illness; and (iii) inability to provide consent or adhere to treatment. Prior to initiating anti-PD-1/L1 antibody therapy, peripheral blood mononuclear cells were isolated from patient blood samples for flow cytometric analysis of monocytic myeloid-derived suppressor cells (M-MDSCs). Data on irAEs and related clinical information were collected, including time of onset, affected organs, and severity, with a minimum follow-up period of 2 months after the final dose of ICIs. Cancer cachexia was defined, according to an international consensus statement,[17] as weight loss of >5% over the past 6 months or a body mass index (BMI) of <20 kg/m^2.

2.7. Hematoxylin–eosin (HE) staining

Mouse organs were harvested and fixed in 4% paraformaldehyde, embedded in paraffin, sectioned, and stained with HE (Servicebio, Wuhan, China). Images were acquired using TissueFAXS SL Spectra (TissueGnostics, Vienna, Austria) and Pannoramic MIDI (Budapest, Hungary).

2.8. Immunofluorescence analysis

Immunofluorescence analysis was performed after antigen retrieval. Sections were microwaved (800 W, low power) in 10 mmol/L citric acid (TTCA Co., Ltd, Anqiu, Shandong, China) for 2 min at high power, followed by 5 min at 50% power. The sections were then cooled for 60 min at 25 °C, washed in PBS, and blocked with 0.5% BSA/PBS for 30 min at 37 °C. Sections were incubated with primary antibodies (Supplemental Table 2) overnight for 12 h at 4 °C and then for 30 min at 37 °C. After washing in PBS, sections were incubated with 1:400 diluted goat/donkey anti-rat Alexa Fluor 488 (Abcam, Cambridge, UK), goat/donkey anti-rabbit Alexa Fluor 594 (Abcam, Cambridge, UK), or goat/donkey anti-mouse Alexa Fluor 647 (Abcam, Cambridge, UK) secondary antibodies for 45 min at 37 °C. Finally, sections were washed and mounted with DAPI (Mounting Medium with DAPI-Aqueous, #ab104139, Abcam, Cambridge, MA, USA) and stored in the dark at −30 °C until imaging. Identical confocal settings were used to limit the intra-experimental variability. Fluorescent signals were detected using a laser scanning confocal microscope and automatic slide slice scan (Leica STELLARIS STED, Wetzlar, Germany). For quantification of the immunofluorescence results, images of the indicated tissues were analyzed using Leica Application Suite X 1.8.0.13313. Alternatively, the absolute number of positive cells/mm^2 in nine fields of interest was statistically analyzed. The investigators were blinded to the experimental groups while conducting the studies.

2.9. Flow cytometry analysis and sorting

After anesthesia with pentobarbital sodium (Chensheng Biotechnology Co., Ltd., Guangzhou, China) solution and cervical dislocation, the thymus was isolated from the anterior mediastinum of each mouse. Thymic lobes were digested enzymatically using 0.25 mg/mL papain (Worthington Biochemical Corp., Lakewood, NJ, USA), 0.25 mg/mL collagenase IV (Roche Life Science, Penzberg, Germany), and 0.1 mg/mL DNase I (Roche Life Science). Single-cell suspensions were obtained from the thymus of mice as described previously.[18,19] The cells were stained with monoclonal antibodies (Supplemental Table 2). For intracellular staining of FoxP3, a FoxP3/Transcription Factor Staining Buffer Kit

(MultiSciences Biotech Co., Ltd, Hangzhou, China) was used following the manufacturer's instructions. Cell phenotypes were evaluated using CytoFLEXLX (Beckman Coulter, Brea, CA, USA). The data were analyzed with the CytExpert and FlowJo V10.0.7 (FlowJo, Ashland, OR, USA). A BD FACSAria III cell sorter (BD Biosciences, Franklin Lakes, NJ, USA) was used for flow cytometry sorting.

2.10. $CD3^+$ T lymphocyte transfer

$CD3^+$ T lymphocytes were isolated via magnetically activated cell sorting (EasySep™ Cell Separation, Stemcell, Vancouver, Canada) from the tumors or spleens of tumor-bearing mice with cachexia or tumor-free mice. Next, 1.5×10^6 $CD3^+$ T lymphocytes were transferred into tumor-free mice via caudal vein injection. After 12 h, the mice were sacrificed, and their lungs, liver, stomach, small intestine, thyroid, skin, salivary glands, pancreas, brain, and eyes were dissected and placed in 4% paraformaldehyde for preservation. These organs were cut into 4-mm sections and stained with HE for microscopic evaluation.

2.11. Caspase activity and nitric oxide (NO) analysis

M-MDSCs were collected to measure the production of NO in the indicated conditioned media and the activity of caspase-3 using a Nitric Oxide Content Assay Kit (Beijing Boxbio Science & Technology, Beijing, China) and Caspase-3 Activity Detection Kit (Beijing Boxbio Science & Technology, Beijing, China), respectively.

2.12. Quantitative reverse transcription-polymerase chain reaction of inducible NO synthase (iNOS)

M-MDSCs were collected, processed using TRIzol reagent (Invitrogen, Carlsbad, CA, USA) to extract total RNA, and then reverse transcribed from 1 μg of total RNA to cDNA using the PrimeScript®RT reagent Kit (TaKaRa Biomedical Technology, Beijing, China), following the manufacturer's instructions. Premix Ex Taq™ (Probe qPCR, TaKaRa Biomedical Technology) was used to perform real-time quantitative assays. The relevant primer sequences used in the experiment are shown as follows: NOS2 (iNOS) forward, 5′-CACCTTGGAAGAGGAGCAAC-3′, NOS2 (iNOS) reverse, 5′-AAGGCCAAACACAGCATACC-3'; GAPDH forward, 5′-AACTTTGGCATTGTGGAAGG-3′, GAPDH reverse, 5′-ACACATTGGGGGTAGGAACA-3'.

2.13. Enzyme-linked immunosorbent assay (ELISA)

Supernatants from the T-cell and M-MDSC co-culture systems and the plasma of patients and donors were collected. Interferon-gamma (IFN-γ) quantification in the supernatants was determined through ELISA (Human IFN Gamma ELISA Kit, Thermo Fisher Scientific, Waltham, MA, USA) following the manufacturer's instructions. Color development is induced by adding a substrate solution. Optical density values are converted to concentrations using a standard curve. Each sample is analyzed in triplicate, and the mean value is used for data interpretation.

2.14. T-cell proliferation and activation assay

T-cell proliferation was determined using the 5,6-carboxyfluorescein diacetate succinimidyl ester (CFSE; Thermo Fisher Scientific, Waltham, MA, USA) dilution assay. Briefly, a freeze-dried powder of CFSE (500 μg, Thermo Fisher Scientific) was dissolved in 180 μL of anhydrous dimethyl sulfoxide (Yoshida Biotechnology Co., Ltd., Beijing, China) and frozen at −30 °C. T-cells were sorted from patients with cancer and healthy donors, labeled with CFSE, and cultured alone or with M-MDSCs at different ratios (2:1, 4:1, 8:1) for 3 days. The cells were then stained for surface marker expression with CD4-FITC (BioLegend, San Diego, CA, USA) or CD8-APC antibodies (BioLegend, Supplemental Table 2); T-cell proliferation was analyzed using a flow cytometer (Beckman Coulter, Brea, CA, USA). Where indicated, 1 mmol/L L-arginine (Cayman Chemicals, Ann Arbor, Michigan, USA), 0.5 mmol/L nor-NOHA (arginase I specific inhibitor; Cayman Chemicals), or 100 μmol/L L-NMMA (inducible NO synthase (iNOS) inhibitor; Cayman Chemicals), was added to the culture on day 0.

2.15. Detection of apoptosis

Annexin V-APC/7-AAD Apoptosis Kit (MultiSciences Biotech Co., Ltd, Hangzhou, China) was used to evaluate the apoptotic death of cells induced by the eluate of test compounds. The assay was prepared in 12-well plates by adding 500 μL of complete medium (with a cell density of 1×10^5 cells/well) and 500 μL of the prepared eluate, followed by incubation for 24 h and 48 h. Cells treated with served as the positive control. The negative control consisted of cells suspended in complete medium and incubated for 24 h and 48 h. Subsequently, the cells were washed twice with cold PBS, and then double-stained using Annexin V-APC (as a marker for early cell death) and 7-aminoactinomycin D (7-AAD; as a marker for cell membrane disruption, necrosis, and late apoptosis). The percentage of apoptotic cells was calculated by flow cytometry using a CytoFLEX flow cytometer (Beckman Coulter, Brea, CA, USA).

2.16. Statistical analysis

GraphPad Prism 9 software (GraphPad Software, La Jolla, CA, USA) was used for data analysis. For comparisons between two groups, either the Student's *t*-test or the Mann–Whitney *U* test was applied, depending on the normality of data distribution. Comparisons involving more than two groups were performed using the Friedman test, one-way ANOVA, or two-way ANOVA, with appropriate corrections for multiple comparisons. A P value of <0.05 was considered statistically significant.

3. Results

3.1. Infiltration of activated T cells parallels thymic atrophy in cachexic HCC mice

To investigate the role of T-cell infiltration in multiple organs in the development of irAEs in advanced cancer, an orthotopic HCC model was established. T-cell infiltration was assessed in tumor-bearing mice exhibiting 5%–10% weight loss, skeletal muscle mass loss, and fat loss (cachexic) and compared with that in non-cachexic tumor-bearing mice and tumor-free controls (Supplemental Fig. 1). Pathological evaluation revealed inflammatory cell infiltration in multiple organs of cachexic HCC mice but not in non-cachexic or tumor-free mice (Fig. 1A and B). Immunofluorescence analysis confirmed infiltration of $CD4^+$ and $CD8^+$ T cells in multiple organs of cachexic HCC mice, whereas few $CD4^+$ or $CD8^+$ T cells were observed in the organs of non-cachexic HCC mice or tumor-free controls (Fig. 1C).

Thymic atrophy was also observed in cachexic HCC mice. Thymus volume, weight, and total cell count were lower in cachexic HCC mice than in non-cachexic HCC mice and tumor-free controls (Fig. 1D). HE staining revealed degradation of the thymic medulla in cachexic HCC mice (Fig. 1E).

Similar findings were observed in 1-year-old cachexic HCC mice (Supplemental Fig. 2). Additionally, because Hepa1-6 is a

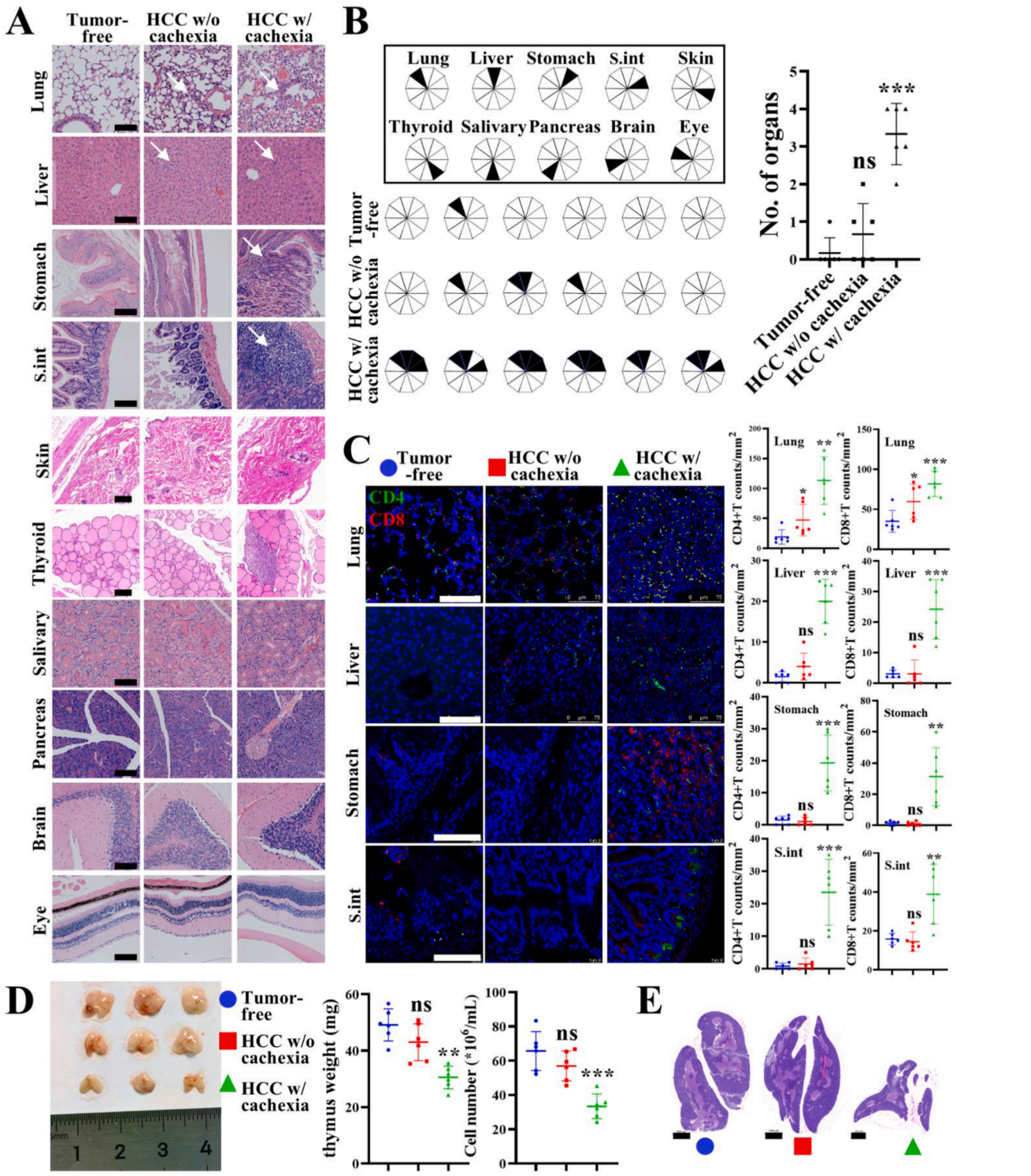


Fig. 1. Infiltration of activated T cells corresponds with thymic involution in cachexic HCC mice. (A, B) Inflammatory cell infiltration in the lungs, liver, stomach, small intestine (S. int), skin, thyroid, salivary glands, pancreas, brain, and eyes of in situ HCC mice that lost <5% (HCC without cachexia, HCC w/o cachexia group) or 5%–10% (HCC with cachexia, HCC w/ cachexia group) of body weight. Sham-operated mice were used as tumor-free controls. Representative HE staining images (A) and decagons depicting inflammation in each organ for individual mice (B) are shown ($n = 6$). Scale bars, 100 μm. Each pie chart represents inflammation status in the listed organs for a single mouse. **(C)** Immunofluorescence staining for $CD4^+$ and $CD8^+$ T cells in the lungs, liver, stomach, and small intestine. Scale bars, 100 μm. **(D)** Representative gross anatomy images of thymus glands and statistical analysis of thymus weight and total cell counts ($n = 6$; two-way ANOVA). (E) Representative HE staining of thymus glands. $^*P < 0.05$, $^{**}P < 0.01$, $^{***}P < 0.001$ (HCC w/o cachexia group *vs.* tumor-free group, HCC w/ cachexia group *vs.* HCC w/o cachexia group); ns, not significant. Abbreviations: HCC, hepatocellular carcinoma; HE, hematoxylin–eosin.

syngeneic tumor for the C57L/J background, thymic atrophy was further evaluated in an in situ HCC model using C57L/J mice, which yielded consistent results (Supplemental Fig. 3). Notably, Hepa1-6 cells formed tumors and spontaneous metastases after implantation in syngeneic C57L/J mice, making it difficult to assess inflammation in tumor-free organs.

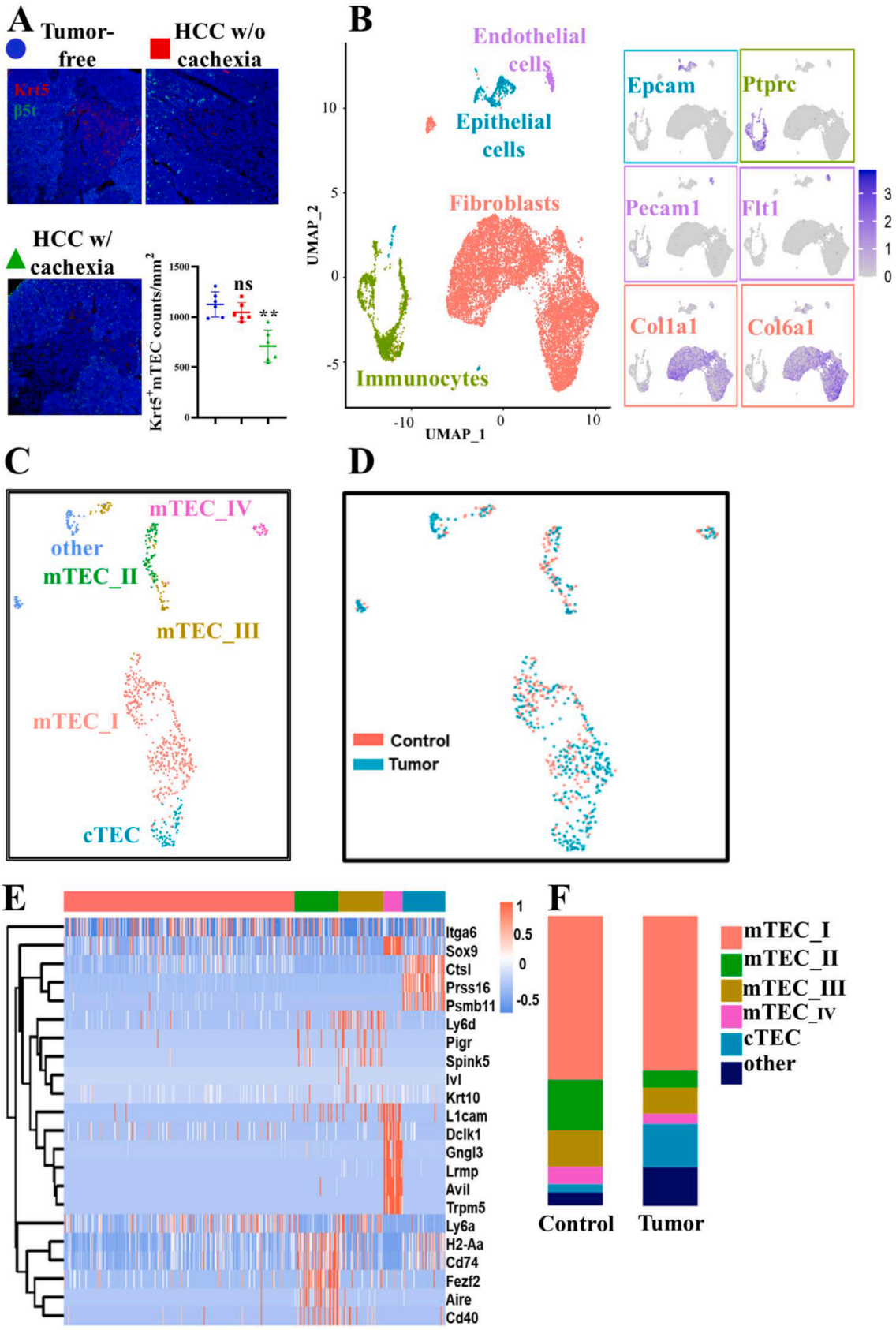


Fig. 2. mTEC abundance is decreased in the involuted thymuses of cachexic mice with HCC. (A) Immunofluorescence staining of Krt5 and β5T in thymic cells. Scale bars, 100 μm. $^{**}P < 0.01$ (HCC w/o cachexia group *vs.* tumor-free group, HCC w/ cachexia group *vs.* HCC w/o cachexia group); ns, not significant. **(B)** Two-dimensional graphical representation of 6531 single cells from six tumor-free mice and 7046 from six cachexic HCC mice, classified into four cell types: endothelial cells, epithelial cells, fibroblasts, and immunocytes; kernel density projection of differentially expressed genes is overlaid. **(C)** Two-dimensional graphical representation of TECs classified into five subsets. **(D)** Distribution of TECs from tumor-free mice and cachexic HCC mice. **(E)** Expression of selected marker genes across the five TEC subsets. **(F)** Distribution of TEC subsets in tumor-free and cachexic HCC mice. Abbreviations: HCC, hepatocellular carcinoma; mTEC, medullary thymic epithelial cell.

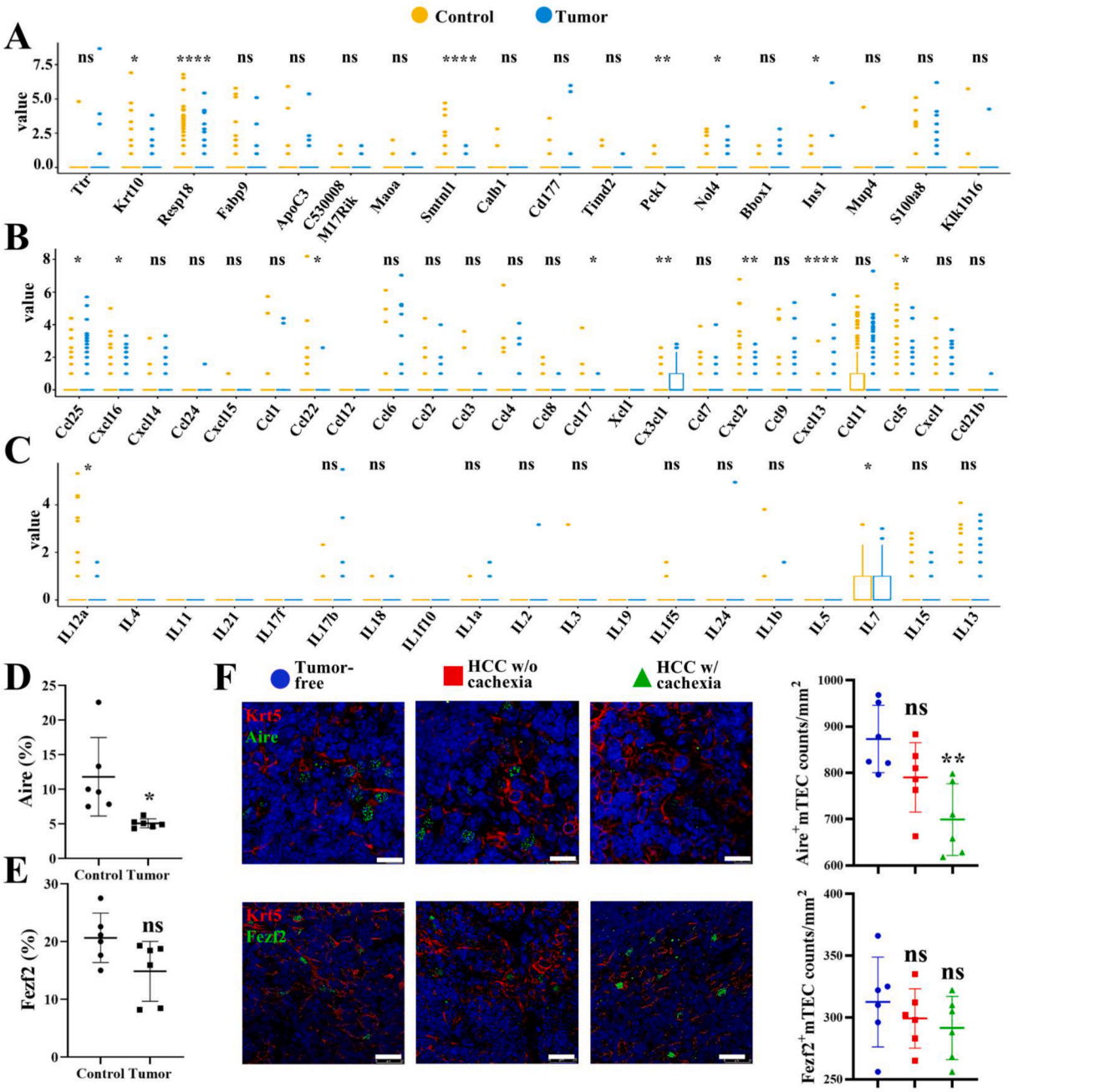


Fig. 3. *Aire* downregulation is accompanied by decreased expression of tissue-restricted antigens (TRAs) in mTECs. (A–C) Relative expression of TRAs (A), chemokines (B), and cytokines (C) in mTECs from tumor-free mice and HCC mice with cachexia. **(D)** Relative expression of *Aire* in mTECs from each tumor-free mouse and cachexic HCC mouse based on scRNA-seq data ($n = 6$, paired *t*-test). **(E)** Relative expression of *Fezf2* in mTECs from each tumor-free mouse and cachexic HCC mouse based on scRNA-seq data ($n = 6$, paired *t*-test). **(F)** Representative images and statistical analyses of immunofluorescence staining for Krt5 and Aire or Fezf2 in thymuses from tumor-free mice and HCC mice with or without cachexia (HCC w/o cachexia group *vs*. tumor-free group, HCC w/ cachexia group *vs*. HCC w/o cachexia group). Scale bars, 25 μm. $^{*}P < 0.05$, $^{**}P < 0.01$, $^{****}P < 0.0001$; ns, not significant. Abbreviations: Aire, autoimmune regulator; Fezf2, Fez family zinc finger 2; HCC, hepatocellular carcinoma; mTECs, medullary thymic epithelial cells.

To explore the relationship between tumor volume, T-cell infiltration, and thymic medulla integrity, subcutaneous HCC and malignant melanoma mouse models were constructed. Tumor growth was limited to a maximum diameter of 1.5 cm, in accordance with humane endpoint criteria, as weight loss was not significant compared with tumor-free mice. In these subcutaneous tumor models, neither T-cell infiltration nor thymic involution was observed (Supplemental Fig. 4).

3.2. mTEC abundance is decreased in the thymuses of cachexic HCC mice

Several cell types in the thymus were evaluated using flow cytometry (Supplemental Fig. 5A). HCC mice with or without cachexia exhibited similar proportions of thymocyte subpopulations, including double-negative ($CD4^{-}CD8^{-}$), double-positive ($CD4^{+}CD8^{+}$), single-positive ($CD4^{+}CD8^{-}$ and

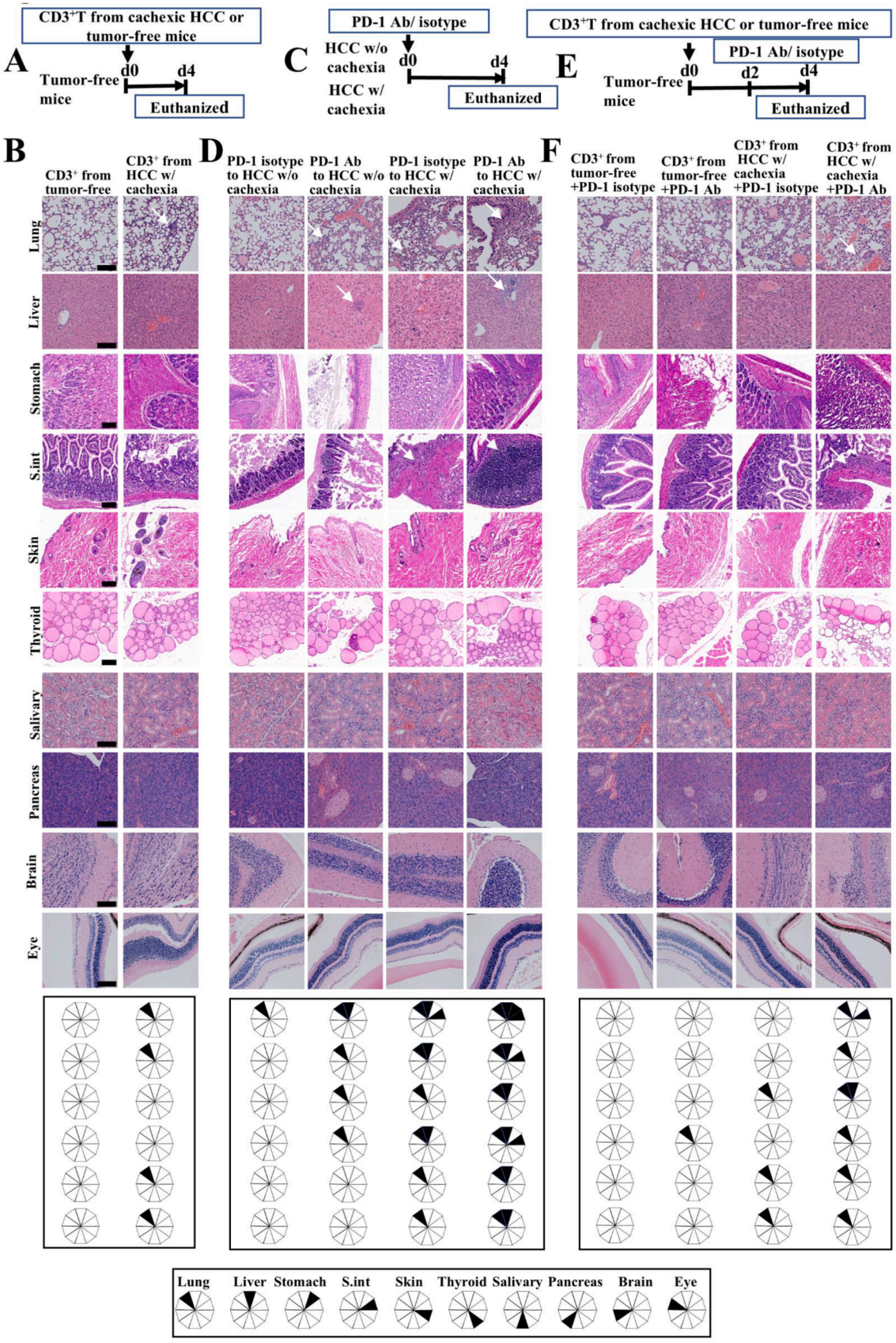


Fig. 4. T cells responsive to TRAs in cachexic HCC mice promote irAEs. (A, B) Tumor-free mice were transferred with $CD3^+$ T cells isolated from the spleen and circulation of cachexic HCC or tumor-free mice. Inflammatory cell infiltration in the lungs, liver, stomach, small intestine (S. int), skin, thyroid, salivary glands, pancreas, brain, and eyes was assessed by HE staining (A). Representative HE staining images and decagons representing individual mice are shown (B, $n = 6$). **(C, D)** HCC mice with or without cachexia were

$CD4^-CD8^+$), mature ($CD3^+CD4^+CD8^-$ and $CD3^+CD4^-CD8^+$), and memory ($CD4^+CD8^-CD44^{high}CD62L^{low}$ and $CD4^-CD8^+CD44^{high}CD62L^{low}$) T cells (Supplemental Fig. 5B). However, the absolute numbers of double-negative, double-positive, CD4 single-positive, CD8 single-positive, and $CD3^+CD4^+$ T cells were decreased in cachexic HCC mice (Supplemental Fig. 5C). Additionally, the proportion of regulatory T cells (Tregs) was higher in the thymuses of cachexic mice than in those of non-cachexic HCC mice, although the absolute cell numbers were similar (Supplemental Fig. 5B and C).

T-cell selection occurs through interactions between thymocytes and TECs.[20] Cortical TECs (cTECs) mediate positive selection, whereas mTECs are responsible for negative selection.[21] Immunofluorescence analysis revealed that Krt5, a marker of mTECs,[22] was significantly less abundant in the thymuses of cachexic HCC mice, whereas β5T, a marker of cTECs,[23] remained unaffected (Fig. 2A and Supplemental Fig. 6). Flow cytometry further confirmed a reduced proportion of mTECs among total TECs in cachexic HCC mice (Supplemental Fig. 5D). Additionally, the proportion of mature mTECs among the total mTECs was decreased (Supplemental Fig. 5D). These findings indicate that HCC-related cachexia is associated with developmental dysregulation of mTECs.

scRNA-seq was performed on $CD45^-$ cells from the thymuses of tumor-free and cachexic HCC mice to investigate the mechanism underlying mTEC involution (Fig. 2B). The analysis focused on TEC subsets classified as cTECs and mTECs: mTEC I (putative TEC progenitors, characterized by high *Itga6* and *Sca1* expression), mTEC II (mature mTECs, with high expression of *Aire*, *Fezf2*, *Cd40*, *H2-Aa*, or *Cd74*), mTEC III (heterogeneous TECs including putative post-AIRE cells, expressing distinct genes such as *Pigr*, *Ly6d*, *Spink5*, *Ivl*, and *Krt10*), and mTEC IV (lacking classical mTEC or cTEC markers but expressing unique genes such as *Lrmp*, *Avil*, *Trpm5*, *Dclk1*, *Gng13*, *L1cam*, and *Sox9*) (Fig. 2C–E).[24] mTECs ectopically express and cross-present a wide array of TRAs, whose expression is stochastic and AIRE-dependent. In cachexic HCC mice, levels of mTEC II and III were decreased, whereas the proportion of cTECs increased significantly (Fig. 2F). These findings indicate that mTEC-driven T-cell negative selection may be dysregulated in cachexic HCC mice.

3.3. Aire downregulation is accompanied by decreased TRAs expression in mTECs

mTECs that ectopically express peripheral TRAs eliminate T cells that strongly recognize these antigens. The expression of TRAs in mTECs is primarily regulated by two independent factors: *Fezf2* and *Aire*.[22,25] Restricted TRA expression can lead to inflammatory cell infiltration, including lymphocytes, in multiple organs.[22] scRNA-seq data revealed that the expression levels of several TRAs in mTECs from cachexic HCC mice were lower than those observed in mTECs from tumor-free mice (Fig. 3A).

Several chemokines and cytokines that may contribute to T-cell negative selection were also significantly altered in the mTECs of cachexic HCC mice compared with those of tumor-free mice, potentially limiting mTEC maturation (Fig. 3B and C). *Aire* expression was downregulated in the mTECs of cachexic HCC mice (Fig. 3D), a finding further confirmed by immunofluorescence analysis (Fig. 3F). Conversely, no difference in *Fezf2* expression was observed between the two groups (Fig. 3E and F).

mTECs in cachexic HCC mice exhibited distinct gene expression profiles compared with those in tumor-free mice, including increased expression of *Ly6a* (Sca1), *Cxcl12*, *Pltp*, *S100a11*, and *Dcn* (Supplemental Fig. 7A). KEGG pathway analysis indicated that the antigen processing and presentation pathway and the apoptosis pathway may be activated in the mTECs of cachexic HCC mice (Supplemental Fig. 7B). Gene Ontology analysis (Supplemental Fig. 7C) further identified the apoptotic signaling pathway, chemokine activity, and chemokine receptor binding as the most enriched terms.

3.4. T cells responsive to the TRAs of cachexic HCC mice promote irAEs

To confirm that TRA-responsive T cells mediate inflammatory cell infiltration in multiple organs, $CD3^+$ T cells from tumor-free mice or cachexic HCC mice were transferred into tumor-free recipient mice (Fig. 4A). $CD3^+$ T cells from cachexic HCC mice led to T-cell infiltration in multiple organs within 4 days post-transfer, indicating that tumor burden did not influence lymphocyte infiltration in tumor-free organs (Fig. 4B, Supplemental Fig. 8A, and Supplemental Fig. 9). Next, an anti-mouse PD-1 antibody or its isotype control was administered to cachexic and non-cachexic HCC mice, and inflammation in tumor-free organs was evaluated after 4 days (Fig. 4C). The anti-PD-1 antibody increased the incidence of inflammation in the tumor-free organs of HCC mice compared with the isotype control (Fig. 4D, Supplemental Fig. 8B, and Supplemental Fig. 9). Furthermore, the incidence of inflammation in tumor-free organs was higher in cachexic HCC mice than in non-cachexic HCC mice (Fig. 4D). However, this experiment did not rule out the potential impact of irAEs development on tumor burden in the liver. To further confirm that TRA-responsive T cells mediated irAEs, $CD3^+$ T cells from the spleens and circulation of cachexic HCC or tumor-free mice were intravenously injected into tumor-free recipient mice, followed by administration of either anti-PD-1 antibody or isotype control on day 2 (Fig. 4E). Mice receiving $CD3^+$ T cells from cachexic HCC mice and treated with anti-PD-1 antibody exhibited the highest incidence of inflammatory cell infiltration in multiple organs (Fig. 4F, Supplemental Fig. 8C, and Supplemental Fig. 9). Mouse weights within and between groups were similar (Supplemental Fig. 8D). Moreover, tumor-free mice that received T cells isolated from the lungs of cachexic HCC mice developed lung inflammation, indicating that T cells infiltrating tumor-free organs in cachexic HCC mice may be TRA-specific (Supplemental Fig. 10).

3.5. M-MDSCs induce mTEC apoptosis through NO production

As previously reported, M-MDSCs are enriched in the thymus of hepatitis B virus (HBV)-infected mice and exert their immunosuppressive effects through NO, which induces apoptosis in various cell types.[26,27] Results from gene set enrichment analysis of apoptosis-related genes, along with Annexin V-APC/7-AAD staining, confirmed that apoptosis occurred in mTECs in cachexic HCC mice (Fig. 5A–C and Supplemental Fig. 11–13). Based on these findings, we postulated that tumor-associated M-MDSCs induce apoptosis in mTECs.

treated with anti-mouse PD-1 antibody (10 mg/kg, clone RMP1-14, Bio X Cell, administered via intraperitoneal injection) or isotype control, and inflammatory cell infiltration in multiple organs was assessed via HE staining (C). Representative HE staining images and decagons representing individual mice are shown (D, $n = 6$). **(E, F)** Tumor-free mice injected with $CD3^+$ T cells from the spleen and circulation of cachexic HCC or tumor-free mice were administered anti-mouse PD-1 antibody or isotype control. Inflammatory cell infiltration in multiple organs was assessed (E), and representative HE staining images with decagons representing individual mice are shown (F, $n = 6$). Scale bars, 100 μm. Abbreviations: HCC, hepatocellular carcinoma; HE, hematoxylin–eosin; irAEs, immune-related adverse events; PD-1, programmed cell death protein 1; TRAs, tissue-restricted antigens.

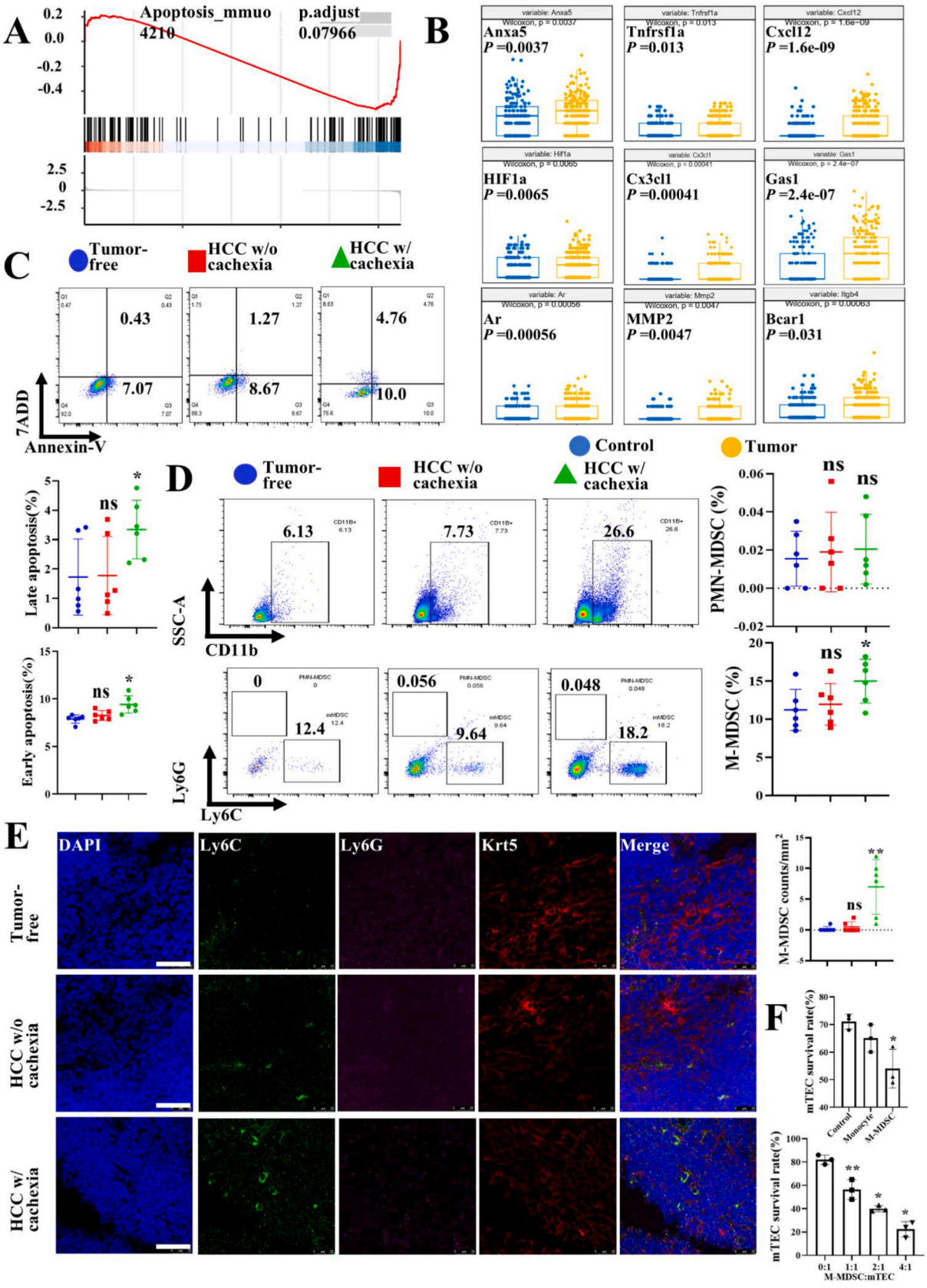


Fig. 5. M-MDSCs induce mTEC apoptosis through NO production. **(A, B)** Gene set enrichment analysis of apoptosis-related gene expression in mTECs from cachexic HCC mice and tumor-free mice. **(C)** Annexin V-APC/7-AAD apoptosis analysis of mTECs ($n = 6$, two-way ANOVA) (HCC w/o cachexia group *vs*. tumor-free group, HCC w/ cachexia group *vs*. HCC w/o cachexia group). **(D)** Flow cytometry analysis of M-MDSCs ($CD11b^{+}Ly6C^{high}Ly6G^{-}$) in the thymus ($n = 6$, two-way ANOVA) (HCC w/o cachexia group *vs*. tumor-free group, HCC w/ cachexia group *vs*. HCC w/o cachexia group). **(E)** Immunofluorescence analysis of Ly6C, Ly6G, and Krt5 in the thymus (HCC w/o cachexia group *vs*. tumor-free group, HCC

Thymic M-MDSC enrichment was observed in cachexic HCC mice, as demonstrated via flow cytometry (Fig. 5D) and immunofluorescence (Fig. 5E) analyses. Thymic M-MDSCs suppressed T-cell proliferation (Supplemental Fig. 14). Furthermore, M-MDSCs from cachexic HCC mice were co-cultured with mTECs isolated from tumor-free mice, and the survival rates of mTECs were recorded. M-MDSCs were found to promote mTEC death in a dose-dependent manner (Fig. 5F and Supplemental Fig. 15A). Additionally, caspase-3 activity was increased in the supernatant of the co-culture system in an M-MDSC dose-dependent manner (Supplemental Fig. 15B).

M-MDSCs induced early apoptosis in mTECs (Supplemental Fig. 15C). Furthermore, *iNOS* expression and NO production were elevated in M-MDSCs from cachexic HCC mice compared with those from tumor-free mice (Supplemental Fig. 15D and E). NO levels in the supernatant of the co-culture system increased in a dose-dependent manner with M-MDSC concentration (Supplemental Fig. 15F). The apoptosis-inducing effect of M-MDSCs on mTECs was inhibited by the iNOS inhibitor L-NMMA, as demonstrated by increased mTEC survival, reduced apoptosis, and decreased caspase-3 activity (Supplemental Fig. 15G–I). Overall, these findings indicate that M-MDSCs induce mTEC apoptosis via NO production.

3.6. M-MDSCs cause thymus atrophy and autoimmune T-cell infiltration in normal organs

We hypothesized that M-MDSCs induce mTEC apoptosis, leading to autoimmune T-cell infiltration in normal organs. To test this, splenic M-MDSCs from cachexic HCC mice, splenic monocytes from tumor-free mice, or PBS were intravenously administered to healthy mice every 3 days for 3 weeks. Infiltration of inflammatory cells in multiple organs and thymic involution were then assessed. Inflammatory cell infiltration (mainly T cells) was observed in mice treated with M-MDSCs but not in those treated with monocytes (Supplemental Fig. 16A and Supplemental Fig. 17). Similarly, thymic atrophy was consistently observed in mice treated with M-MDSCs but not in those treated with monocytes, as indicated by reduced thymus volume, weight, and cell number (Fig. 6A), degradation of the thymic medulla (Fig. 6B), and flow cytometry showing reduced mTECs and mature mTECs (Fig. 6C). The body weights of mice did not change following M-MDSC or monocyte transfer (Supplemental Fig. 18A).

The anti-Ly6C antibody or its isotype control was administered intravenously every 3 days to target M-MDSCs, beginning 1 week after establishing the HCC mouse model. This treatment resulted in a reduction in M-MDSC numbers (Fig. 6D and Supplemental Fig. 19), milder thymic involution (Fig. 6E and F, and Supplemental Fig. 16B), and an increase in mTEC abundance. These findings were supported by immunofluorescence staining for β5T and Krt5 (Supplemental Fig. 16C) as well as flow cytometry analysis of mTECs and mature mTECs (Supplemental Fig. 16D). Consequently, depletion of M-MDSCs suppressed inflammatory cell infiltration in multiple organs (Supplemental Fig. 16E and F) without affecting the body weights of the mice (Supplemental Fig. 18B).

3.7. Cancer cachexia-related M-MDSCs predict irAEs occurrence in patients with cancer receiving ICIs

Sixty-four patients with advanced cancer receiving ICI treatment were included in this study (Supplemental Table 1), of whom 38 experienced irAEs. Patients who developed irAEs exhibited higher levels of circulating M-MDSCs than those without irAEs (Fig. 7A). Moreover, patients with cachexia (defined as BMI <20 kg/m^2 or ≥5% weight loss over the past 6 months) had elevated M-MDSC levels (Fig. 7A). Kaplan–Meier failure function analysis showed no significant association between high M-MDSC levels (above the median), low BMI, or ≥5% weight loss and the overall occurrence of irAEs (Fig. 7B and C) or initial treatment response (Supplemental Fig. 20). However, the duration of ICI treatment was positively associated with the development of irAEs (Supplemental Fig. 21). Notably, patients with both high M-MDSC levels and low BMI or ≥5% weight loss experienced a higher incidence of irAEs (hazard ratio: 2.333; 95% confidence interval: 1.231–4.423) (Fig. 7C). Furthermore, M-MDSCs isolated from patients with cancer suppressed T-cell activation in a dose-dependent manner (Fig. 7D). High level of *iNOS* expression was observed (Supplemental Fig. 22A). Treatment with L-NMMA, an iNOS inhibitor, mitigated the immunosuppressive effects of M-MDSCs (Supplemental Fig. 22B and C). These findings suggest that M-MDSCs in patients with advanced cancer induce NO production and may serve as predictive markers for irAEs occurrence.

4. Discussion

Activation of lymphocytes responsive to TRAs is a key mechanism in the development of autoimmune diseases and irAEs.[8,9] mTECs play a central role in the negative selection of T cells, which is primarily responsible for eliminating autoreactive T cells.[28,29] Tregs and lymphatic endothelial cells in lymph nodes also contribute to the negative selection process.[30] Thymic involution, which begins in adulthood, increases the likelihood of dysfunction in negative selection.[31] However, under normal physiological and certain pathological conditions, immune checkpoints help restrain the activation of autoreactive lymphocytes, thereby preventing the onset of autoimmune diseases. T-cell infiltration of normal organs has been observed in the context of thymic involution, particularly in elderly individuals.[32] Despite this, predicting the occurrence, affected organs, and severity of irAEs remains challenging and often appears stochastic.[2] Importantly, TRA expression in mTECs follows a stochastic pattern and is primarily regulated by the transcription factors AIRE and FEZF2.[22,25] Given that administration of ICIs to patients with thymic tumors is associated with severe irAEs,[33] thymic dysfunction may be a contributing factor in irAE development. In the present study, we observed thymic atrophy in cachexic tumor-bearing mice. Furthermore, mTEC dysfunction impaired the negative selection of T cells, resulting in autoimmune T-cell infiltration into normal, tumor-free organs.

Cachexia-associated thymic atrophy contributed to the development of irAEs. Infiltration of tissues by activated T cells is widely recognized as a hallmark of irAEs.[34] Additionally, activation of B cells, humoral immune responses, and the formation of tertiary lymphoid structures have also been implicated in irAEs pathogenesis.[35] The activation of autoreactive lymphocytes represents a central mechanism underlying irAEs. Tumor antigens and undiagnosed pre-existing autoimmune conditions may also contribute to their development.[36] Peripheral tolerance mechanisms mediated by Tregs and extrathymic AIRE-expressing cells may help control irAEs onset and severity.[37] In the present study, we demonstrated that expansion of the autoreactive T-cell pool due to thymic atrophy in cachexic cancer-bearing hosts does not fully account for the development of irAEs. Additionally, several clinical

w/ cachexia group *vs.* HCC w/o cachexia group). Scale bars, 100 μm. **(F)** Survival of mTECs co-cultured with the indicated cell types and ratios ($n = 3$, two-way ANOVA) (M-MDSC group *vs.* Monocyte group) (1:1 group *vs.* 0:1 group, 2:1 group *vs.* 1:1 group, 4:1 group *vs.* 2:1 group). $^{*}P < 0.05$, $^{**}P < 0.01$; ns, not significant. Abbreviations: 7-AAD, 7-aminoactinomycin D; HCC, hepatocellular carcinoma; M-MDSCs, monocytic myeloid-derived suppressor cells; mTEC, medullary thymic epithelial cell; NO, nitric oxide.

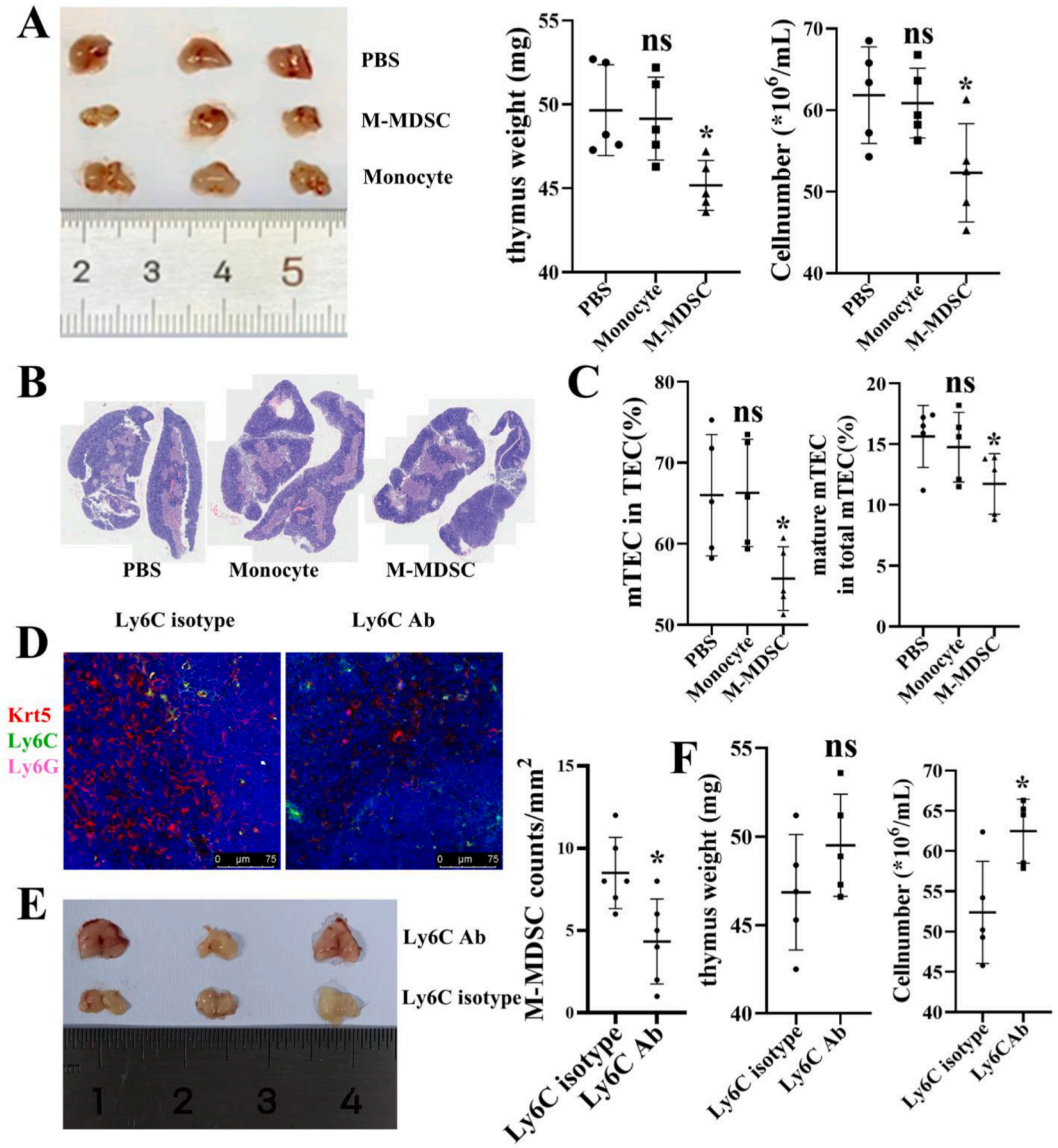


Fig. 6. M-MDSCs cause thymus involution and autoimmune T-cell infiltration in normal organs. (A) Representative images of thymus gland gross anatomy and statistical analysis of thymus weights and absolute cell numbers ($n = 5$, two-way ANOVA) (Monocyte group *vs.* PBS group, M-MDSC group *vs.* Monocyte group). **(B)** Representative HE staining of the thymus gland. **(C)** Statistical analysis of mTECs and mature mTECs in mice ($n = 5$, two-way ANOVA) (Monocyte group *vs.* PBS group, M-MDSC group *vs.* Monocyte group). **(D)** Immunofluorescence analysis of Ly6C and Krt5 in the thymus of HCC mice treated with anti-Ly6C antibody or isotype control. Scale bars, 100 μm. Statistical analyses are shown. **(E, F)** Representative thymus gland gross anatomy and corresponding statistical analysis of thymus weights and absolute cell numbers ($n = 5$). $^{*}P < 0.05$; ns, not significant. Abbreviations: Ab, antibody; HCC, hepatocellular carcinoma; HE, hematoxylin–eosin; M-MDSCs, monocytic myeloid-derived suppressor cells; mTECs, medullary thymic epithelial cells; PBS, phosphate-buffered saline.

features apart from cachexia-associated thymic atrophy are likely to be involved in irAEs susceptibility.

The involuted thymus leads to reduced output of naïve T cells, a limited T-cell receptor repertoire, relatively enhanced Treg cell generation, induction of immunosenescence, and potential suppression of immune surveillance of neoplasia. Aside from age, acute thymic atrophy can also be induced by several infectious agents (including bacteria, viruses, parasites, and fungi) as well as other factors such as stress, pregnancy, malnutrition, chemotherapy, and cancer.[38,39] This study revealed that cancer-related cachexia causes thymic atrophy, which leads to dysfunction in T-cell negative selection. In particular, during ICI treatment, several factors, including chemotherapy, infection, and unresolved malnutrition, can induce thymic atrophy and increase the incidence of irAEs. Although this study demonstrated the predictive value of pretreatment M-MDSC levels and weight loss for irAEs occurrence, dynamic predictive models incorporating weight loss, M-MDSCs, and other thymic insults are needed to improve the accuracy of irAEs prediction.

MDSCs and certain cytokines may contribute to cancer cachexia–associated thymic atrophy. In mTECs from cachexic tumor-bearing mice, levels of CCL25, CX3CL1, and CXCL13 were elevated, whereas those of CXCL16, CCL22, CCL17, CXCL2, and CCL5 were decreased. CCL25 in the thymus is known to chemoattract dendritic cells (DCs).[40] $CD3^{+}NK1.1^{-}TCR\beta^{+}CD4^{-}CD8^{-}$ double-negative T cells enhance Treg cell recruitment via CCL5 in ischemic stroke lesions.[41] Transendothelial DCs chemoattracted by the endothelial ligand CX3CL1 may facilitate the thymus in acquiring blood-borne antigens to induce and maintain central tolerance.[42] However, the precise roles of these altered cytokines

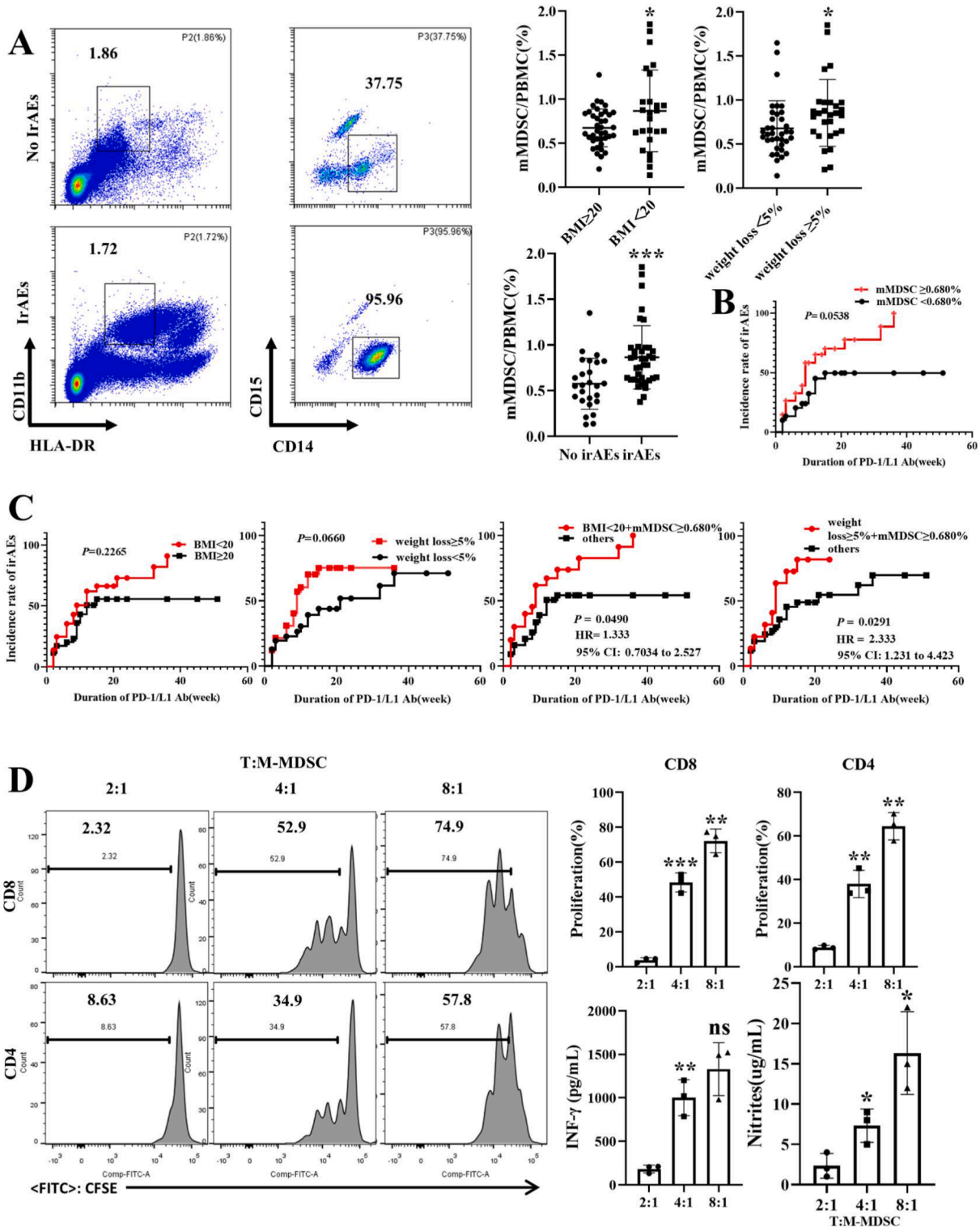


Fig. 7. Cancer cachexia-related M-MDSCs predict irAE occurrence in patients with cancer receiving ICIs. (A) Flow cytometry analysis of circulating M-MDSCs in 64 patients with advanced cancer before ICI treatment. Statistical analysis of M-MDSC levels among patients with or without irAEs, BMI <20 kg/m^2, or weight loss ≥5% was performed. **(B, C)** Kaplan–Meier failure function illustrating the cumulative incidence of irAEs in patient subgroups. **(D)** Suppressive activity of M-MDSCs from cachexic patients with HCC on the proliferation of circulating T cells stimulated with anti-CD3/anti-CD28. Representative flow cytometry plots, statistical analysis, IFN-γ levels, and NO levels are shown ($n = 3$ biologically independent samples, two-way ANOVA) (4:1 group *vs.* 2:1 group, 8:1 group *vs.* 4:1 group). $^{*}P < 0.05$, $^{**}P < 0.01$, $^{***}P < 0.001$; ns, not significant. Abbreviations: BMI, body mass index; HCC, hepatocellular carcinoma; ICI, immune checkpoint inhibitor; IFN-γ, interferon-gamma; irAEs, immune-related adverse events; M-MDSCs, monocytic myeloid-derived suppressor cells; NO, nitric oxide; PD-1/L1, programmed cell death protein 1/ligand 1.

and chemokines in T-cell negative selection remain unclear and warrant further investigation. MDSCs are immunosuppressive and tumor-promoting cells that also play roles in various inflammatory diseases.[43,44] Indeed, MDSC accumulation is associated with the severity of inflammatory diseases, whereas MDSC transfer has been reported to alleviate several autoimmune diseases.[45,46] In the

present study, however, M-MDSC transfer did not alleviate T-cell infiltration in normal organs. In contrast, Fang *et al.*[26] reported that M-MDSC chemoattraction to the thymus in chronic hepatitis B induces central tolerance to HBV by presenting HBV antigens to thymocytes. We confirmed infiltration of tumor-associated M-MDSCs into the corticomedullary junction of the thymus and demonstrated their novel role in inducing mTEC apoptosis through NO production, a mechanism also observed in various other cell types.[47] Nonetheless, the impact of limited M-MDSC production on the efficacy of ICI treatments in elderly patients requires further investigation.

The causes of cancer-associated cachexia include, at a minimum, tumor progression and systemic inflammation. Several murine tumor models, both spontaneous and experimentally induced, have been used to study cancer cachexia; however, a single tumor model cannot fully reproduce the heterogeneity of human cancers. The primary hallmark of cancer cachexia is the loss of skeletal muscle mass, accompanied by progressive functional impairment, reduced food intake (anorexia), and body weight loss. In the present study, we employed in situ HCC-related cachexia models, which exhibited skeletal muscle and body weight loss. Reduced physical activity and food intake were also observed. Thus, the variation in cachexia development among in situ HCC mice was attributed to differences in tumor progression and systemic inflammation. Cachexic HCC mice consistently exhibited a greater tumor burden than non-cachexic counterparts. Furthermore, previous studies on the role of MDSCs in cancer have shown that M-MDSC transfer generally promotes tumor progression. Based on this, we speculated that the transfer of cancer cachexia–associated M-MDSCs could also contribute to tumor progression. Notably, subcutaneous models of HCC and melanoma, in which tumors reached the ethical limit of 1.5 cm in diameter, did not result in cachexia. In contrast, in situ HCC tumors of similar size consistently led to cachexia. These findings indicate that thymic atrophy in cachexic HCC mice may result from both tumor progression and cachexia. However, our study does not rule out the possibility that thymic destruction could be mediated by autoimmune attack during the process of thymic atrophy. Additionally, whether cachexia resulting from other causes follows a similar biological mechanism warrants further investigation.

In the current study, mTEC dysfunction during thymic atrophy induced by cancer-associated cachexia was characterized by a decreased total number of mTECs, a relatively lower proportion of mature mTECs, and reduced expression of *Aire* within mTECs. M-MDSCs induced apoptosis of mTECs, which may be a critical factor contributing to their dysfunction. Accordingly, we speculate that M-MDSCs play a fundamental role in thymic atrophy associated with cancer cachexia. Although mTECs primarily direct the negative selection of T cells, Tregs and fibroblasts also contribute to this process to some extent.[48] The number of Tregs increased during thymic involution, which may have further contributed to impaired T-cell negative selection and warrants additional investigation.

In this study, the Hepa1-6 cell line-based model effectively simulates orthotopic HCC. The Hepa1-6 model, serving as a homologous transplantation model, exhibits rapid tumor growth over a matter of weeks, with cachexia manifesting in its advanced stages. It primarily mimics the consumption resulting from tumor burden alone, but falls short in replicating the backdrop of chronic liver injury, persistent inflammation, and metabolic disturbances. Virus models, such as those involving HBV transgenic animals, boast a pathological progression that aligns more closely with human conditions, potentially offering a superior simulation of metabolic disturbances and systemic inflammation. Nevertheless, these models are encumbered by extended construction cycles, high costs, and potentially insignificant cachexia phenotypes. The chemical induction model, utilizing diethylnitrosamine (DEN)/CCL4, stands out for its prominent chronic liver injury characteristics. However, it is plagued by significant interindividual variability and random tumor localization, which may compromise experimental consistency. Furthermore, the chemicals employed may harbor systemic toxicity, necessitating careful differentiation between drug toxicity and cachexia.

This study also has some limitations. The causal relationship between thymic atrophy and infiltration of TRA-responsive T cells requires further validation, potentially through transplantation of atrophied thymuses into healthy recipients. Such a procedure may reverse thymic involution and result in minimal infiltration of TRA-responsive T cells into normal organs. Additionally, the timing and severity of irAEs could not be predicted based on the findings of this study. Therefore, further research, particularly involving human samples, is needed to clarify the role of thymic atrophy in the development of irAEs.

5. Conclusions

In conclusion, thymic atrophy was observed in cachexic tumor-bearing mice. Impaired thymic T-cell negative selection, caused by mTEC dysfunction, led to autoimmune T-cell infiltration into normal organs, serving as a prerequisite for the development of irAEs. Furthermore, cancer cachexia–associated M-MDSCs were found to induce mTEC apoptosis during thymic atrophy and may serve as predictive biomarkers for irAE development.

Authors' contributions

Li Wei: Writing – original draft, Visualization, Validation, Software, Writing – review & editing, Methodology, Investigation, Formal analysis, Data curation. **Ya-Qin Sun:** Writing – original draft, Visualization, Validation, Software, Resources, Writing – review & editing, Methodology, Investigation. **Jian-Hua Ren:** Validation, Methodology, Investigation, Formal analysis, Data curation, Writing – original draft, Writing – review & editing. **Ze-Xuan Huang:** Resources, Methodology. **Yuan Zhang:** Visualization, Validation, Project administration, Methodology. **Xiu-Qing Pang:** Visualization, Resources, Methodology. **Xiao-Tong Lv:** Validation, Software, Resources. **Xiang-Yuan Wu:** Supervision, Project administration, Funding acquisition, Conceptualization. **Yan-Fang Xing:** Supervision, Project administration, Funding acquisition, Conceptualization. **Xing Li:** Writing – original draft, Supervision, Resources, Project administration, Funding acquisition, Conceptualization.

Data availability statement

All data generated and/or analyzed during this study are available from the corresponding authors upon reasonable request.

Declaration of competing interest

The authors declare that there is no conflicts of interest.

Acknowledgements

This study was supported by the National Natural Science Foundation of China (No. 82170749), the Guangdong Basic and Applied Basic Research Foundation (No. 2022A1515010465 and 2022A1515012659), Guangzhou Science and Technology Program

Key Projects (No. 2023B01J1007), and the Traditional Chinese Medicine Bureau of Guangdong Province, China (No. 20241045).

Appendix A. Supplementary data

Supplementary data to this article can be found online at https://doi.org/10.1016/j.livres.2025.10.001.

References

1. Waldman AD, Fritz JM, Lenardo MJ. A guide to cancer immunotherapy: from T cell basic science to clinical practice. *Nat Rev Immunol*. 2020;20:651–668. https://doi.org/10.1038/s41577-020-0306-5.
2. Martins F, Sofiya L, Sykiotis GP, et al. Adverse effects of immune-checkpoint inhibitors: epidemiology, management and surveillance. *Nat Rev Clin Oncol*. 2019;16:563–580. https://doi.org/10.1038/s41571-019-0218-0.
3. Owen CN, Bai X, Quah T, et al. Delayed immune-related adverse events with anti-PD-1-based immunotherapy in melanoma. *Ann Oncol*. 2021;32:917–925. https://doi.org/10.1016/j.annonc.2021.03.204.
4. Salem JE, Manouchehri A, Moey M, et al. Cardiovascular toxicities associated with immune checkpoint inhibitors: an observational, retrospective, pharmacovigilance study. *Lancet Oncol*. 2018;19:1579–1589. https://doi.org/10.1016/S1470-2045(18)30608-9.
5. Kang JH, Bluestone JA, Young A. Predicting and preventing immune checkpoint inhibitor toxicity: targeting cytokines. *Trends Immunol*. 2021;42:293–311. https://doi.org/10.1016/j.it.2021.02.006.
6. Chennamadhavuni A, Abushahin L, Jin N, Presley CJ, Manne A. Risk factors and biomarkers for immune-related adverse events: a practical guide to identifying high-risk patients and rechallenging immune checkpoint inhibitors. *Front Immunol*. 2022;13:779691. https://doi.org/10.3389/fimmu.2022.779691.
7. Won T, Kalinoski HM, Wood MK, et al. Cardiac myosin-specific autoimmune T cells contribute to immune-checkpoint-inhibitor-associated myocarditis. *Cell Rep*. 2022;41:111611. https://doi.org/10.1016/j.celrep.2022.111611.
8. Benesova K, Kraus FV, Carvalho RA, et al. Distinct immune-effector and metabolic profile of CD8+ T cells in patients with autoimmune polyarthritis induced by therapy with immune checkpoint inhibitors. *Ann Rheum Dis*. 2022;81:1730–1741. https://doi.org/10.1136/ard-2022-222451.
9. Lozano AX, Chaudhuri AA, Nene A, et al. T cell characteristics associated with toxicity to immune checkpoint blockade in patients with melanoma. *Nat Med*. 2022;28:353–362. https://doi.org/10.1038/s41591-021-01623-z.
10. Setiawan T, Sari IN, Wijaya YT, et al. Cancer cachexia: molecular mechanisms and treatment strategies. *J Hematol Oncol*. 2023;16:54. https://doi.org/10.1186/s13045-023-01454-0.
11. Ouyang Z, Tao WL, Yu SY, Zou M. Advances in pharmacotherapies in cancer-related cachexia. *Oncol Transl Med*. 2023;9:15–21. https://doi.org/10.1007/s10330-022-0611-1.
12. Bossi P, Delrio P, Mascheroni A, Zanetti M. The spectrum of malnutrition/cachexia/sarcopenia in oncology according to different cancer types and settings: a narrative review. *Nutrients*. 2021;13:1980. https://doi.org/10.3390/nu13061980.
13. Rich NE, Phen S, Desai N, et al. Cachexia is prevalent in patients with hepatocellular carcinoma and associated with worse prognosis. *Clin Gastroenterol Hepatol*. 2022;20:e1157–e1169. https://doi.org/10.1016/j.cgh.2021.09.022.
14. Ainiwaer A, Cheng J, Lang R, et al. Chinese expert consensus on the clinical application of molecular diagnostics in hepatobiliary cancers (2024 edition). *Liver Res*. 2024;8:195–206. https://doi.org/10.1016/j.livres.2024.11.005.
15. Chowdhrya SM, Chowdhry VK. Cancer cachexia and treatment toxicity. *Curr Opin Support Palliat Care*. 2019;13:292–297. https://doi.org/10.1097/SPC.0000000000000450.
16. Zhang WL, Li N, Shen Q, et al. Establishment of a mouse model of cancer cachexia with spleen deficiency syndrome and the effects of atractylenolide I. *Acta Pharmacol Sin*. 2020;41:237–248. https://doi.org/10.1038/s41401-019-0275-z.
17. Fearon K, Strasser F, Anker SD, et al. Definition and classification of cancer cachexia: an international consensus. *Lancet Oncol*. 2011;12:489–495. https://doi.org/10.1016/S1470-2045(10)70218-7.
18. Kim MJ, Serwold T. Isolation of highly viable thymic epithelial cells for use in in vitro and in vivo experiments. *Methods Mol Biol*. 2019;1899:143–156. https://doi.org/10.1007/978-1-4939-8938-6_11.
19. Ohigashi I, Takahama Y. Flow cytometry analysis of thymic epithelial cells and their subpopulations. *Methods Mol Biol*. 2016;1323:65–73. https://doi.org/10.1007/978-1-4939-2809-5_5.
20. Karimi MM, Guo Y, Cui X, et al. The order and logic of CD4 versus CD8 lineage choice and differentiation in mouse thymus. *Nat Commun*. 2021;12:99. https://doi.org/10.1038/s41467-020-20306-w.
21. Robey E, Fowlkes BJ. Selective events in T cell development. *Annu Rev Immunol*. 1994;12:675–705. https://doi.org/10.1146/annurev.iy.12.040194.003331.
22. Takaba H, Morishita Y, Tomofuji Y, et al. Fezf2 orchestrates a thymic program of self-antigen expression for immune tolerance. *Cell*. 2015;163:975–987. https://doi.org/10.1016/j.cell.2015.10.013.
23. Ohigashi I, Takahama Y. Specific impact of β5t on proteasome subunit composition in cortical thymic epithelial cells. *Cell Rep*. 2021;36:109657. https://doi.org/10.1016/j.celrep.2021.109657.
24. Bornstein C, Nevo S, Giladi A, et al. Single-cell mapping of the thymic stroma identifies IL-25-producing tuft epithelial cells. *Nature*. 2018;559:622–626. https://doi.org/10.1038/s41586-018-0346-1.
25. Nishijima H, Matsumoto M, Morimoto J, et al. Aire controls heterogeneity of medullary thymic epithelial cells for the expression of self-antigens. *J Immunol*. 2022;208:303–320. https://doi.org/10.4049/jimmunol.2100692.
26. Fang Z, Zhang Y, Zhu Z, et al. Monocytic MDSCs homing to thymus contribute to age-related CD8+ T cell tolerance of HBV. *J Exp Med*. 2022;219:e20211838. https://doi.org/10.1084/jem.20211838.
27. Zhang Y, Xu B, Luan B, et al. Myeloid-derived suppressor cells (MDSCs) and mechanistic target of rapamycin (mTOR) signaling pathway interact through inducible nitric oxide synthase (iNOS) and nitric oxide (NO) in asthma. *Am J Transl Res*. 2019;11:6170–6184.
28. Coder BD, Wang H, Ruan L, Su DM. Thymic involution perturbs negative selection leading to autoreactive T cells that induce chronic inflammation. *J Immunol*. 2015;194:5825–5837. https://doi.org/10.4049/jimmunol.1500082.
29. Shi Y, Zhu M. Medullary thymic epithelial cells, the indispensable player in central tolerance. *Sci China Life Sci*. 2013;56:392–398. https://doi.org/10.1007/s11427-013-4482-4.
30. Cohen JN, Guidi CJ, Tewalt EF, et al. Lymph node-resident lymphatic endothelial cells mediate peripheral tolerance via Aire-independent direct antigen presentation. *J Exp Med*. 2010;207:681–688. https://doi.org/10.1084/jem.20092465.
31. Lancaster JN, Keatinge-Clay DE, Srinivasan J, et al. Central tolerance is impaired in the middle-aged thymic environment. *Aging Cell*. 2022;21:e13624. https://doi.org/10.1111/acel.13624.
32. Srinivasan J, Lancaster JN, Singarapu N, Hale LP, Ehrlich LR, Richie ER. Age-related changes in thymic central tolerance. *Front Immunol*. 2021;12:676236. https://doi.org/10.3389/fimmu.2021.676236.
33. Wang W, Lin G, Hao Y, et al. Treatment outcomes and prognosis of immune checkpoint inhibitors therapy in patients with advanced thymic carcinoma: a multicentre retrospective study. *Eur J Cancer*. 2022;174:21–30. https://doi.org/10.1016/j.ejca.2022.06.059.
34. Lozano AX, Chaudhuri AA, Nene A, et al. T cell characteristics associated with toxicity to immune checkpoint blockade in patients with melanoma. *Nat Med*. 2022;28:353–362. https://doi.org/10.1038/s41591-021-01623-z.
35. Dhodapkar KM, Duffy A, Dhodapkar MV. Role of B cells in immune-related adverse events following checkpoint blockade. *Immunol Rev*. 2023;318:89–95. https://doi.org/10.1111/imr.13238.
36. Liu X, Shi Y, Zhang D, et al. Risk factors for immune-related adverse events: what have we learned and what lies ahead? *Biomark Res*. 2021;9:79. https://doi.org/10.1186/s40364-021-00314-8.
37. Michelson DA, Hase K, Kaisho T, Benoist C, Mathis D. Thymic epithelial cells co-opt lineage-defining transcription factors to eliminate autoreactive T cells. *Cell*. 2022;185:2542–2558. https://doi.org/10.1016/j.cell.2022.05.018.
38. Ansari AR, Liu H. Acute thymic involution and mechanisms for recovery. *Arch Immunol Ther Exp (Warsz)*. 2017;65:401–420. https://doi.org/10.1007/s00005-017-0462-x.
39. Wang W, Thomas R, Oh J, Su DM. Thymic aging may be associated with COVID-19 pathophysiology in the elderly. *Cells*. 2021;10:628. https://doi.org/10.3390/cells10030628.
40. Yu H, Mei Y, Dong Y, et al. CCR9-CCL25 mediated plasmacytoid dendritic cell homing and contributed the immunosuppressive microenvironment in gastric cancer. *Transl Oncol*. 2023;33:101682. https://doi.org/10.1016/j.tranon.2023.101682.
41. Tian D, Pan Y, Zhao Y, et al. TCRalphabeta$^+$ NK1.1$^-$CD4$^-$CD8$^-$ double-negative T cells inhibit central and peripheral inflammation and ameliorate ischemic stroke in mice. *Theranostics*. 2023;13:896–909. https://doi.org/10.7150/thno.80307.
42. Vollmann EH, Rattay K, Barreiro O, et al. Specialized transendothelial dendritic cells mediate thymic T-cell selection against blood-borne macromolecules. *Nat Commun*. 2021;12:6230. https://doi.org/10.1038/s41467-021-26446-x.
43. Kumar V, Patel S, Tcyganov E, Gabrilovich DI. The nature of myeloid-derived suppressor cells in the tumor microenvironment. *Trends Immunol*. 2016;37:208–220. https://doi.org/10.1016/j.it.2016.01.004.
44. Cassetta L, Bruderek K, Skrzeczynska-Moncznik J, et al. Differential expansion of circulating human MDSC subsets in patients with cancer, infection and inflammation. *J Immunother Cancer*. 2020;8:e001223. https://doi.org/10.1136/jitc-2020-001223.
45. Xu D, Li C, Xu Y, Huang M, Cui D, Xie J. Myeloid-derived suppressor cell: a crucial player in autoimmune diseases. *Front Immunol*. 2022;13:1021612. https://doi.org/10.3389/fimmu.2022.1021612.
46. Li X, Chen J, Chen YJ, et al. Dexamethasone and lactoferrin induced PMN-MDSCs relieved inflammatory adverse events of anti-cancer therapy without tumor promotion. *Commun Biol*. 2021;4:252. https://doi.org/10.1038/s42003-021-01769-z.
47. González R, Molina-Ruiz FJ, Bárcena JA, Padilla CA, Muntané J. Regulation of cell survival, apoptosis, and epithelial-to-mesenchymal transition by nitric oxide-dependent post-translational modifications. *Antioxid Redox Signal*. 2018;29:1312–1332. https://doi.org/10.1089/ars.2017.7072.
48. Nitta T, Tsutsumi M, Nitta S, et al. Fibroblasts as a source of self-antigens for central immune tolerance. *Nat Immunol*. 2020;21:1172–1180. https://doi.org/10.1038/s41590-020-0756-8.